Hindawi Publishing Corporation
International Journal of Photoenergy
Volume 2012, Article ID 874509, 8 pages
doi:10.1155/2012/874509

Research Article

Fabrication of Al-Doped TiO_2 Visible-Light Photocatalyst for Low-Concentration Mercury Removal

Cheng-Yen Tsai,[1] Tien-Ho Kuo,[2] and Hsing-Cheng Hsi[3]

[1] *Graduate Institute of Engineering Science and Technology, National Kaohsiung First University of Science and Technology, No. 2 Jhuoyue Road, Nanzih, Kaohsiung 811, Taiwan*
[2] *Department of Environmental, Safety, and Health Engineering, Tungnan University, Section 3, 152, Peishen Road, Shenkeng, New Taipei 222, Taiwan*
[3] *Institute of Environmental Engineering and Management, National Taipei University of Technology, Section 3, No. 1, Chung-Hsiao E. Road, Taipei 106, Taiwan*

Correspondence should be addressed to Hsing-Cheng Hsi, hchsi@ntut.edu.tw

Received 13 September 2011; Revised 30 December 2011; Accepted 31 December 2011

Academic Editor: Gongxuan Lu

High-quality Al-doped TiO_2 visible-light photocatalyst was prepared via a single-step direct combination of vaporized Ti, Al, and O_2 using a 6 kW thermal plasma system. Results showed that the formed Al-doped TiO_2 nanoparticles were a mixture of anatase and rutile phase and had a size between 10 and 105 nm. The absorption spectra of the nanoparticles shifted towards the visible light regions, depending on the Al_2O_3 addition. Ti^{4+} and Ti^{3+} coexisted in the synthesized Al-doped TiO_2; the Ti^{3+} concentration, however, increased with increasing Al_2O_3 addition due to Al/Ti substitution that caused the occurrence of oxygen vacancy. Hg^0 breakthrough tests revealed that the nanoparticles had an appreciable Hg^0 removal under visible-light irradiation. Nevertheless, moisture reduced Hg removal by the nanoparticles, especially when visible-light irradiation was applied, suggesting that the competitive adsorption between H_2O and Hg species on the active sites of TiO_2 surface occurred.

1. Introduction

Mercury (Hg) releases from nature and anthropogenic sources have been the major focus of environmental studies owing to the toxicity and bioaccumulative behaviors [1]. Hg species in gaseous phase from emission sources in general exist in three main forms: elemental (Hg^0), oxidized (Hg^{2+}), and particle-bound (Hg_p). Hg^{2+} and Hg_p can be easily removed by air pollution control devices such as wet flue gas desulfurization and electrostatic precipitators. Nevertheless, Hg^0 is highly volatile, insoluble in water, and thus difficult to remove from a gas stream.

Using titanium dioxide (TiO_2) photocatalysts as adsorbents and catalysts has been advised as a novel technique to effectively remove Hg^0 [2–11]. Wu et al. [2] used in situ produced TiO_2 particles to remove Hg under UV irradiation. Upon irradiation with UV light, active sites become available on the TiO_2 particle surface and effectively adsorbed Hg to form a complex with TiO_2. The manufacturing procedures strongly influence the purity and surface characteristics of resulting TiO_2 nanoparticles, which afterward affect the photocatalytic properties. Sol-gel method has been widely used in the bench-scale TiO_2 nanoparticles fabrication due to its simplicity to perform [12–15]. Nevertheless, the processing temperature of sol-gel method syntheses is relatively low. A multistep fabrication procedure, that is, sample synthesis and subsequent calcination, was thus needed to transform the obtained TiO_2 into anatase or rutile. Thermal plasma has been shown to possess advantages to develop nanoparticles with clean surface and narrow particle size distribution. Using thermal plasma as a heating source may directly vaporize Ti metal having a high melting point at 1941 K and induce the high-purity TiO_2 formation in a single step.

A decisive obstruction in the successful application of TiO_2 is the band gap energy of 3.2 eV causing the TiO_2 only being activated by UV irradiation. Visible-light (VL) TiO_2

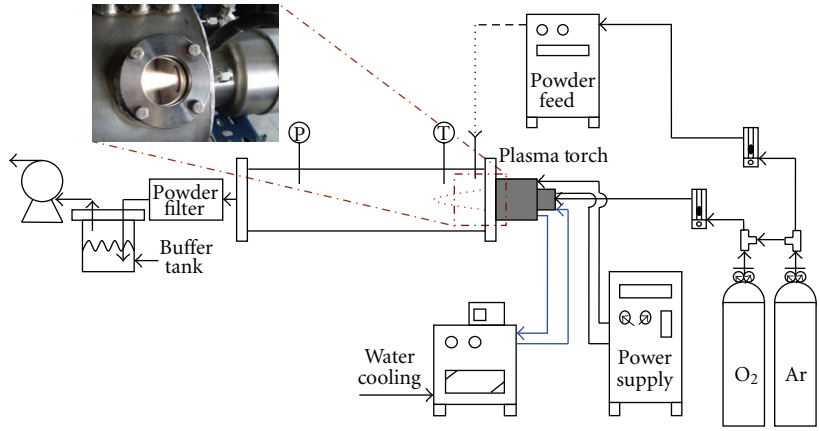

Figure 1: Schematic diagram of non-transferred DC plasma torch system for synthesis Al-doped TiO_2 photocatalysts.

photocatalysts have therefore obtained great attention in recent years. Several studies have indicated that an improved TiO_2 photocatalyst excited by VL sources can be prepared by substitutional doping with metal atoms, such as Fe [16, 17], Er [18], and Al [19–23]. Because the ionic radii for Al and Ti are similar (0.053 nm for Al^{3+} and 0.061 nm for Ti^{4+}), Al can easily fill into a regular cation position and form a substitutional solid solution. Numerous studies have shown that Al-doped TiO_2 nanoparticles can be manufactured via vapor-phase. Lee et al. [19] prepared Al-doped TiO_2 with thermal plasma using $TiCl_4$ and $AlCl_3$ as precursors. The absorption band of synthesized Al-doped TiO_2 nanoparticles shifted from the UV region to the VL region. Choi et al. [23] prepared Al-doped TiO_2 nanoparticles using a citrate-nitrate autocombustion system with Ti solution and $Al(NO_3)_3$ solution as precursors. The authors also demonstrated that Al-doped TiO_2 gas sensor was more selective and sensitive to CO and O_2 under 600°C.

In our previous study, high-purity TiO_2 nanoparticles using Ti metal as a precursor were successfully manufactured with a transferred plasma torch [24]. Nevertheless, using transferred DC plasma torch as the heating source has defects on low nanoparticles yield. Another plasma system was established in our earlier study using a nontransferred DC plasma torch as the heating source [25]. Our preliminary test has shown that Al-doped TiO_2 nanoparticles can be successfully formed in a single step via this non-transferred DC thermal plasma system. However, the anatase/rutile ratio of the formed Al-doped TiO_2 was below 58.2 wt%, which may be due to the higher plasma power (i.e., 8 kW). In this study, Al-doped TiO_2 photocatalyst with a broad absorption spectrum was developed under a lower plasma power (i.e., 6 kW). The photocatalyst fabricated from this innovative single-step procedure was tested for Hg^0 capture under both UV and VL irradiation. We expected that a reducing plasma power can increase the anatase ratio of the formed Al-doped TiO_2 crystal. The greater content of anatase phase in TiO_2 may enhance the transformation of Hg^0 into Hg^{2+}, which could subsequently enhance the removal effectiveness of TiO_2. The Hg^0 removal effectiveness of Al-doped TiO_2 in the presence of O_2, H_2O, and light irradiation was further discussed. Notably, few studies have examined the VL photocatalytic effects of Al-doped TiO_2 on removal of Hg^0 at an extreme low concentration, namely, $\mu g\ Nm^{-3}$ level.

2. Experimental Details

2.1. Synthesis of Al-Doped TiO_2 Nanoparticles. The DC plasma torch apparatus used for preparing TiO_2 nanoparticles is illustrated in Figure 1. The system comprised a non-transferred plasma torch connected to a DC power supply (Model PHS-15C, Taiwan Plasma Corp., Taiwan), a stainless steel reaction chamber (i.d. = 30 cm; length = 100 cm), a stainless steel powder feeder, a powder filter, a buffer tank, and a vacuum pump (GVD-050A, ULVAC) for shifting the particles floating in the exhaust gas. The plasma torch consisted of a water-cooled copper alloy electrode. The system was performed at 30 A and 200 V. Titanium powder (99.8% purity), Al_2O_3 powder (99.9% purity), and ultrahigh-purity (UHP) O_2 were used as precursors. A mixture of UHP Ar and O_2 was used as the plasma gas. The flow rate was 60 L min^{-1} at $Ar : O_2 = 3 : 1$ by volume. UHP Ar with a flow rate of 2 L min^{-1} was also used as the carrier gas of the Ti and Al_2O_3 powder feedstock. The Al_2O_3/Ti mass ratio was controlled at 0, 0.1, 0.3, and 0.5. The powder feeding rate was fixed at 0.2 g min^{-1}. The gas stream containing the formed TiO_2 nanoparticles was passed through the stainless steel powder filter and a buffer tank induced by the vacuum pump.

2.2. Al-Doped TiO_2 Nanoparticle Characterization. The particle size and morphology of TiO_2 nanoparticles were examined with a transmission electron microscope (TEM, Philips CM-200). Powder X-ray diffraction (XRD, Rigaku Rinet 200) with Cu $\kappa\alpha$ radiation (λ = 1.5405 Å) was used for crystal structure identification. The JCPDS database was used for powder crystalline phase identification. The mass fractions of anatase to rutile in formed TiO_2 nanoparticles were calculated by [26],

$$f_A = \frac{1}{1 + 1.26 I_R / I_A}, \quad (1)$$

where f_A is the mass fraction of anatase, I_A is the intensity of (101) reflection of anatase, and I_R is the intensity of (110) reflection of rutile. The diffuse reflectance UV-visible spectra (UV-Vis) of TiO_2 nanoparticles were measured from 300 to 800 nm using a spectrophotometer (Hitachi U-3010). X-ray photoelectron spectroscopy (XPS, ULVAC-PHI 1600) was used for Ti, O, Al, and Cu bonding patterns identification. The obtained XPS spectra were deconvoluted with the XPSPEAK software.

2.3. Hg Removal Experiments. Al-doped TiO_2 synthesized at the Al_2O_3/Ti mass ratio of 0.5 was evaluated for the removal effectiveness of low-concentration gaseous Hg^0. Gaseous Hg^0 was generated with a certificated Hg^0 permeation tube (VICI Metronics) which heated at 70 ± 0.1°C to ensure a constant Hg^0 diffusion rate. Gaseous Hg^0 with a known concentration was mixed with N_2, O_2, and water vapor which was generated by streaming N_2 passed through a water bubbler. All gas mixing and Hg^0 injection occurred within a temperature-controlled chamber and heated tubes/lines to prevent water condensation. The generated Hg^0-containing gas with a concentration of 10–15 μg Hg^0 Nm^{-3} and a flow rate of 1.5 L min^{-1} flowed through the photochemical reactor with 30 mg Al-doped TiO_2 were irradiated with UV or VL light. The photochemical reactor was a cylindrical quartz tube with an i.d. = 25 mm and a length = 150 mm. The nanoparticles were uniformly coated onto a glass slide, which was placed horizontally in the tube. The UV and VL light sets was located 1 cm above the tube. The photochemical tube reactor was operated at 25°C and atmospheric pressure. The effluent gas from the photochemical reactor flowed through a moisture trap (i.e., a nefion tube) to remove H_2O from the gas stream and thus to minimize the interference in Hg detection. The tail gas then flowed through a gold amalgamation column held by a heating coil (Brooks Rand model AC-01) where the Hg^0 in the gas was adsorbed. The Hg^0 that was concentrated on the gold was then thermally desorbed and sent as a concentrated Hg stream to a cold-vapor atomic fluorescence spectrophotometer (Model III, Brooks Rand Lab) for analysis. Six minutes were needed to complete a test run; ten runs were performed for each test condition. Finally, the exhaust was passed through a carbon trap before it was effluent into the fume hood.

3. Results and Discussion

Figure 2 illustrates the TEM images of the nanoparticles produced at various Al_2O_3/Ti mass ratios. TEM results indicated that the synthesized Al-doped TiO_2 was homogeneous, without significant phase separation or coating on the surface. It was also noticed that the synthesized nanoparticles was in hexagonal or spherical shapes; adding Al_2O_3 powder had insignificant effects on the shape of the formed nanoparticles. The darker areas in the TEM micrographs showed the agglomeration of Al-doped TiO_2 nanoparticles. The powder size of the feedstock Ti and Al_2O_3 powder were about 5–15 μm. However, nanoparticles formed at Al_2O_3/Ti mass ratios of 0 to 0.5 were approximately between 10 and 105 nm. These observation results indicate that the injected Ti and Al_2O_3 powders successfully vaporized at the high flame temperature and subsequently synthesized Al-doped TiO_2 nanoparticles via the recombination of vaporized Ti, O and Al atoms in the thermal plasma environment.

Table 1: Crystal phases of Al-doped TiO_2 synthesized at various Al_2O_3/Ti mass ratio.

Al_2O_3/Ti mass ratio	f_A (wt.%)	Phase detected
0	64.31	Anatase, rutile
0.1	62.67	Anatase, rutile
0.3	59.67	Anatase, rutile
0.5	53.77	Anatase, rutile, Al_2O_3

XRD powder patterns for the nanoparticles fabricated at various Al_2O_3/Ti mass ratios are presented in Figure 3. All the peak intensity of powder diffraction was normalized by anatase (101). The experimental results suggested that most of the diffraction peaks could be designated as the presence of anatase and rutile phases. However, the diffraction peaks standing for Al_2O_3 appeared as Al_2O_3/Ti = 0.5, based on 2θ = 35.15°, 43.35°, 52.5°, and 57.5° that are indexed to the Al_2O_3 diffraction pattern. These observations are consistent with our previous work [25] and suggest that at Al_2O_3/Ti = 0.5 loading, the thermal plasma was less effective to vaporize the Al_2O_3 powders and to induce the interactions between Ti, O, and Al atoms. Moreover, the relative content of anatase, depicted with the f_A value (Table 1), noticeably reduced with increasing Al_2O_3/Ti due to consequent transformation into rutile at an elevating temperature [27]. Notably, the TiO_2 was fabricated at a fixed plasma power of 6 kW. The plasma temperature change at various Al_2O_3/Ti ratios should be small and may not markedly influence the transformation of anatase into rutile. The enhancement in transformation of anatase into rutile may also attribute to the increase in Al doping [19, 21, 22, 28].

Figure 4 demonstrates the UV-visible spectra of the Al-doped TiO_2 nanoparticles synthesized at various Al_2O_3/Ti mass ratios over the wavelength range of 300–800 nm. The commercial Degussa P-25 photocatalyst was also tested for comparison. The experimental results showed that the absorption edge was at ~390 nm for P-25 photocatalyst. The TiO_2 nanoparticles synthesized in thermal plasma at the Al_2O_3/Ti mass ratio of 0 to 0.3 possessed an absorption edge at ~400 nm. The absorption spectra of Al-doped TiO_2 slightly shifted from UV to VL region with reference to an increase in Al_2O_3/Ti mass ration can be assigned to the band gap narrowing relation to the interstitial Al species in the TiO_2 crystal [19, 29, 30]. Especially, TiO_2 synthesized at Al_2O_3/Ti = 0 also had band gap absorption at ~400 nm, which was comparable to that of Al-doped TiO_2 formed at Al_2O_3/Ti = 0.1. The extent of red shift and band broadening may be attributed to the presence of oxygen vacancies in TiO_2 crystal formed in the high-temperature plasma flame. Numerous studies have shown the appearance of the visible-light activity was attributed to the newly formed oxygen vacancy state in the TiO_2 band structure [24, 31]. Further

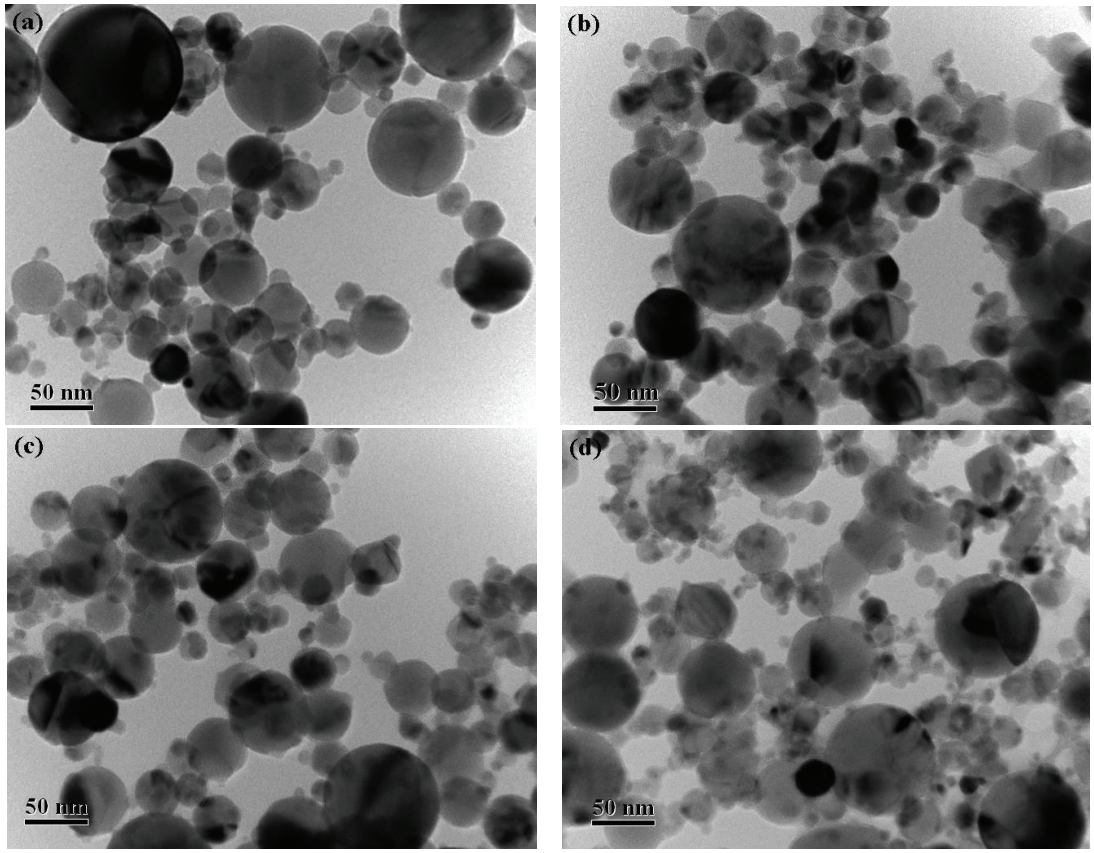

Figure 2: TEM images of TiO_2 nanoparticles synthesized at Al_2O_3/Ti mass ratio of (a) 0, (b) 0.1, (c) 0.3, and (d) 0.5.

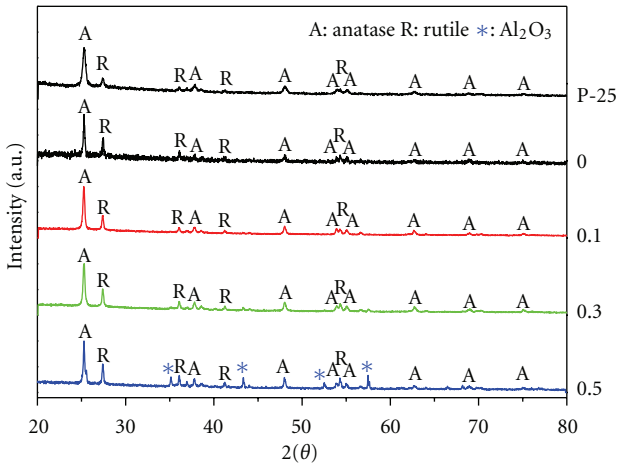

Figure 3: XRD patterns of TiO_2 nanoparticles synthesized at Al_2O_3/Ti = 0 to 0.5 and Degussa P-25.

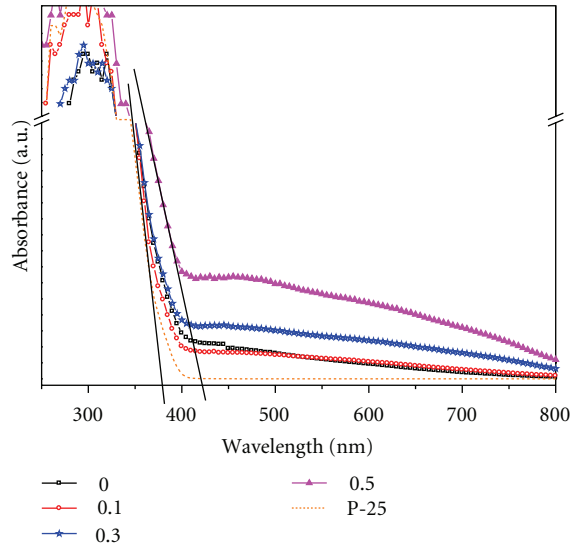

Figure 4: Optical absorption spectra of synthesized Al-doped TiO_2 and commercial P-25 photocatalyst.

evidences and explanation are presented based on XPS analysis. In contrast, the Al-doped TiO_2 synthesized at Al_2O_3/Ti = 0.5 showed strong absorption in the VL range, suggesting that the extent of red shift and broadening was greatly dependent on Al_2O_3 concentrations in the plasma environment.

The XPS spectra of Ti_{2p} for the synthesized TiO_2 nanoparticles are shown in Figure 5. The Al_{2p} spectra for the synthesized TiO_2 nanoparticles at a Al_2O_3/Ti mass ratio of 0.1, 0.3, and 0.5 are shown in Figure 6. The Ti_{2p} XPS spectra acquired from TiO_2 fabricated at various Al_2O_3/Ti mass ratios were deconvoluted into four peaks within 456.4–464.5 eV, including $Ti^{4+}_{2p1/2}$, $Ti^{3+}_{2p1/2}$, $Ti^{4+}_{2p3/2}$, and $Ti^{3+}_{2p3/2}$. These

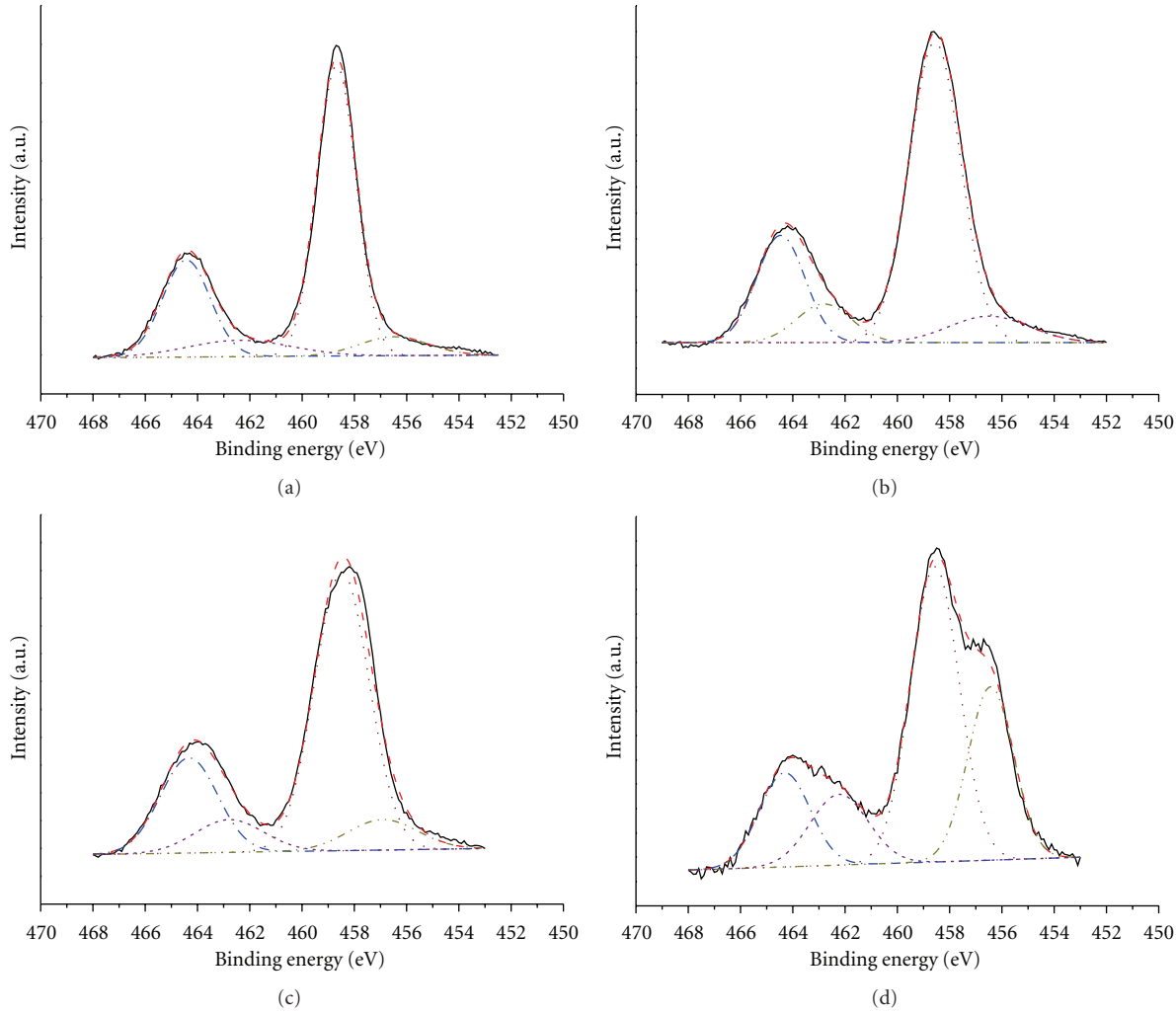

Figure 5: Ti_{2p} XPS spectra of TiO_2 synthesized at Al_2O_3/Ti mass ratio of (a) 0, (b) 0.1, (c) 0.3, and (d) 0.5.

peaks are indications to the presence of TiO_2 ($Ti^{4+}_{2p1/2}$and $Ti^{4+}_{2p3/2}$) and Ti_2O_3 ($Ti^{3+}_{2p1/2}$ and $Ti^{3+}_{2p3/2}$), respectively [32]. For the Al-doped TiO_2, the Al_{2p} peaks at a binding energy of 75.5 eV can be attributed to the presence of Al^{3+}. The results suggested that the Al^{3+} content enhanced with an increase in Al_2O_3 addition. The calculated $Ti^{3+}/(Ti^{3+}+ Ti^{4+})$ ratios for Al-doped TiO_2 at Al_2O_3/Ti = 0, 0.1, 0.3, and 0.5 were 3.1, 17.1, 17.5, and 33.2%, respectively, based on the deconvoluted peak area. These data indicated that Ti^{3+} concentration greatly enhanced with increasing Al_2O_3 addition owing to the transformation of TiO_2 into Ti_2O_3. We suspected that Ti^{4+}/Al^{3+} ionic substitution may take place during the Al doping. If this assumption held, when Ti^{4+} (ionic radius = 0.061 nm) is substituted by Al^{3+} (ionic radius = 0.053 nm) from TiO_2 crystal, the lattice mismatch occurs as a result of that the ionic radius of Ti^{4+} is larger than that of Al^{3+}. To atone for the smaller ionic radius of Al^{3+}, a Ti species having an ionic radius larger than Ti^{4+} is needed. Consequently, Ti^{4+} is reduced to Ti^{3+} (ionic radius = 0.067 nm). The observed Ti^{3+} peaks in the present study are consistent with Steveson et al. [33] and our previous work [25]. In addition, the formal charge generated by the substitution of Ti^{4+} with Al^{3+} can also be compensated via the formation of O^- from O^{2-}, which resulted in the oxygen vacancies found in Al-doped TiO_2 [21, 33, 34].

Table 2: Atomic percentage of synthesized TiO_2 nanoparticles based on XPS examinations.

Al_2O_3/Ti mass ratio	Composition (at.%)			
	O	Al	Ti	Cu
0	74.17	0	23.25	2.57
0.1	65.95	6.77	25.33	1.95
0.3	62.96	10.45	23.13	3.46
0.5	57.83	22.09	15.44	4.63

Notably, about 1.95–4.62 at.% Cu was found in the formed Al-doped TiO_2 based on the XPS analysis (Table 2). The Cu impurity was from the vaporization of plasma torch made of Cu alloy under the high-temperature plasma environment. Associated with the results from the UV-visible

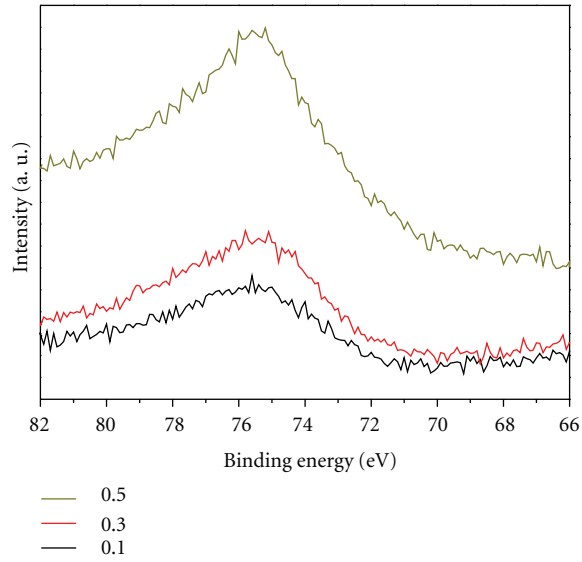

Figure 6: Al_{2p} XPS spectra of TiO_2 produced at Al_2O_3/Ti mass ratio of 0.1, 0.3, and 0.5.

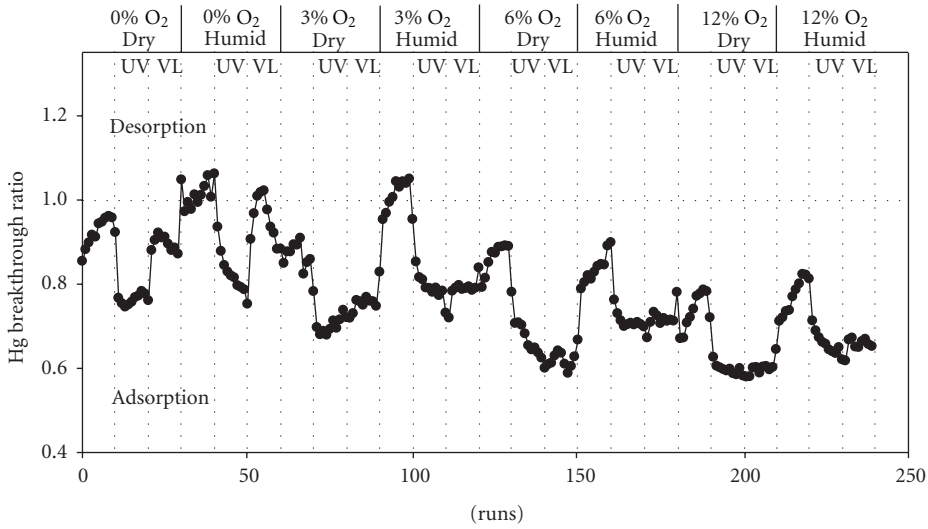

Figure 7: Hg breakthrough ratio of Al-doped TiO_2 in the continuous adsorption experiment under various test conditions.

analysis, the doped Cu and the oxygen vacancy may synergistically contribute to the observed red shift in the UV-visible absorption spectrum for the non-Al-doped TiO_2 (i.e., Al_2O_3/Ti = 0). Nevertheless, Zhang et al. suggested that Cu content < 38 at.% in TiO_2 had negligible effects on the Ti_{2p} binding energy of XPS examinations [35]. Therefore, isomorphous substitution due to Al doping into TiO_2 crystal should be the major contribution of the increasing Ti^{3+}. The red shift in the absorption spectra of TiO_2 nanoparticles thus primarily was attributed to the Al doping and generated oxygen vacancy (Figure 4).

The Hg^0 adsorption breakthrough results for Al-doped TiO_2 nanoparticles synthesized at Al_2O_3/Ti = 0.5 are shown in Figure 7. The experimental parameters included O_2 concentration, humidity, and the type of light sources. These parameters were tested alternately by gradually increasing the O_2 concentration from 0% to 12% combined with introducing H_2O (20% relative humidity) and UV/VL irradiation to the photocatalytic reactor. The experimental results showed that Hg^0 capture was very small with rapid breakthrough at the 0% O_2, dry (H_2O < 0.1 vol%), and dark condition (runs 0–10 in Figure 7), manifesting that the synthesized Al-doped TiO_2 (Al_2O_3/Ti = 0.5) was less effective in removal of Hg^0 under the test condition. This result was anticipated because Hg^0 appeared to the main Hg species at the 0% O_2, dry, and dark condition and was not easy to form a strong binding with the surface of TiO_2. However, an increase in the Hg^0 capture to 25% was apparently observed when UV irradiation was applied (breakthrough down to approximately 0.75; runs 11–20). The significant enhancement in Hg^0 removal for Al-doped TiO_2 nanoparticles under UV irradiation is a strong indication that this sample had

a good photocatalytic potential to transform Hg^0 into Hg^{2+} that enhanced the adsorption onto Al-doped TiO_2. It is also noteworthy that without the presence of O_2, VL was less effective in photocatalytic oxidation than UV (runs 21–30). In addition, a significant decrease in Hg^0 capture was observed at the humid condition (runs 31–60). This result suggest that H_2O competitively adsorbs onto the TiO_2 active sites, causing the reemission of adsorbed Hg species, which can be Hg^0 or Hg^{2+} needed to be further examined. The experimental results presented here are in agreement with those found in earlier studies [6, 7, 24, 36]. Li and Wu reported that the physically adsorbed Hg^0 can be desorbed from the surface of a SiO_2-TiO_2 composite by water vapor at high concentration, which suggested that Hg^0 is only weakly adsorbed on the sorbent surface [6]. Dissimilar to H_2O, O_2 notably improved the adsorption of Hg^0; increasing O_2 concentration strongly enhanced the Hg^0 capture of Al-doped TiO_2 to up to 40% (equivalent to breakthrough of 0.6; Figure 7). It is noteworthy that when O_2 was > 6%, Hg^0 capture was similar for Al-doped TiO_2 under either UV or VL irradiation (runs 131–150 and 221–240). These data not only revealed the importance of O_2 in enhancing Hg^0 capture, but also verified the visible-light activity of the synthesized Al-doped TiO_2 nanoparticles on Hg^0 oxidation/adsorption.

4. Conclusion

Al-doped TiO_2 nanoparticles were successfully synthesized in a single step using Ti powders, Al_2O_3 powders, and O_2 by a nontransferred plasma torch system. TiO_2 nanoparticles formed at Al_2O_3/Ti mass ratios 0 to 0.5 were approximately between 10 and 105 nm. The crystal phases of the formed TiO_2 nanoparticles were mainly in anatase and rutile forms. However, increasing the Al_2O_3 addition caused the ratio of anatase to rutile decreased. The presence of oxygen vacancy and the substitution of Ti^{4+} with Al^{3+} were suspected to cause the slight red shift in the absorption edge to lower energy due to band gap narrowing. Al doping and oxygen vacancy in the TiO_2 crystal may also result in the phase transformation from TiO_2 to Ti_2O_3. Hg breakthrough results showed that the Hg^0 removal with formed Al-doped TiO_2 in a dry condition was greater than that in a humid condition when light irradiation was applied. Hg capture was also found to be markedly enhanced by increasing O_2 concentration. Nevertheless, H_2O showed deteriorating effects on the adsorption of Hg through competition for active sites on the Al-doped TiO_2 surface. Results presented here suggest that Hg^0 removal using synthesized Al-doped TiO_2 nanoparticles may be greatly affected by the extent of catalytic transformation of Hg^0 into Hg^{2+} and amphoteric (hydrophilic-hydrophobic) surface properties of Al-doped TiO_2.

We envision that the photocatalyst can be successfully used to capture Hg from coal-derived flue gas. Nevertheless, it is imperative to note that this study employed gas streams consisting of Hg^0 in a moisture-oxygen-nitrogen mix. Coal-derived flue gas is a complex mixture also containing fly ash particles, moisture, CO, and many acid gases. For example, a typical untreated flue gas derived from the combustion of a US low sulfur eastern bituminous coal can contain 5–7% H_2O, 3-4% O_2, 15-16% CO_2, 1 ppbv total Hg, 20 ppm CO, 10 ppm hydrocarbons, 100 ppm HCl, 800 ppm SO_2, 10 ppm SO_3, 500 ppm NO_x, and balance N_2 [9–11]. The influences of the flue gas components on Hg removal using TiO_2 photocatalysts are thus highly needed to be further investigated.

Acknowledgments

This paper was supported by National Science Council of Taiwan (NSC95-2622-E-327-002-CC3) and Taiwan Plasma Corp., Kaohsiung, Taiwan. The authors acknowledge Mr. Chin-Cheng Ho, Taiwan Plasma Corp. and Dr. Hsunling Bai, National Chiao Tung University, Taiwan, for their technical assistance. The authors also thank the two anonymous reviewers for their valuable comments and suggestions to improve the quality of the paper.

References

[1] E. G. Pacyna, J. M. Pacyna, K. Sundseth et al., "Global emission of mercury to the atmosphere from anthropogenic sources in 2005 and projections to 2020," *Atmospheric Environment*, vol. 44, no. 20, pp. 2487–2499, 2010.

[2] C. Y. Wu, T. G. Lee, G. Tyree, E. Arar, and P. Biswas, "Capture of mercury in combustion systems by in situ-generated titania particles with UV irradiation," *Environmental Engineering Science*, vol. 15, no. 2, pp. 137–148, 1998.

[3] E. Pitoniak, C. Y. Wu, D. Londeree et al., "Nanostructured silica-gel doped with TiO_2 for mercury vapor control," *Journal of Nanoparticle Research*, vol. 5, no. 3-4, pp. 281–292, 2003.

[4] P. Biswas and C. Y. Wu, "Nanoparticles and the environment," *Journal of the Air and Waste Management Association*, vol. 55, no. 6, pp. 708–746, 2005.

[5] E. Pitoniak, C. Y. Wu, D. W. Mazyck, K. W. Powers, and W. Sigmund, "Adsorption enhancement mechanisms of silica-titania nanocomposites for elemental mercury vapor removal," *Environmental Science and Technology*, vol. 39, no. 5, pp. 1269–1274, 2005.

[6] Y. Li and C. Y. Wu, "Role of moisture in adsorption, photocatalytic oxidation, and reemission of elemental mercury on a SiO_2-TiO_2 nanocomposite," *Environmental Science and Technology*, vol. 40, no. 20, pp. 6444–6448, 2006.

[7] Y. Li and C. Y. Wu, "Kinetic study for photocatalytic oxidation of elemental mercury on a SiO_2-TiO_2 nanocomposite," *Environmental Engineering Science*, vol. 24, no. 1, pp. 3–12, 2007.

[8] E. J. Granite, W. P. King, D. C. Stanko, and H. W. Pennline, "Implications of mercury interactions with band-gap semiconductor oxides," *Main Group Chemistry*, vol. 7, no. 3, pp. 227–237, 2008.

[9] E. J. Granite, H. W. Pennline, and J. S. Hoffman, "Effects of photochemical formation of mercuric oxide," *Industrial and Engineering Chemistry Research*, vol. 38, no. 12, pp. 5034–5037, 1999.

[10] E. J. Granite and H. W. Pennline, "Photochemical removal of mercury from flue gas," *Industrial and Engineering Chemistry Research*, vol. 41, no. 22, pp. 5470–5476, 2002.

[11] E. J. Granite, M. C. Freeman, R. A. Hargis, W. J. O'Dowd, and H. W. Pennline, "The thief process for mercury removal from flue gas," *Journal of Environmental Management*, vol. 84, no. 4, pp. 628–634, 2007.

[12] H. Yamashita, M. Harada, J. Misaka, M. Takeuchi, K. Ikeue, and M. Anpo, "Degradation of propanol diluted in water under visible light irradiation using metal ion-implanted titanium dioxide photocatalysts," *Journal of Photochemistry and Photobiology A*, vol. 148, no. 1–3, pp. 257–261, 2002.

[13] C. Di Valentin, G. Pacchioni, A. Selloni, S. Livraghi, and E. Giamello, "Characterization of paramagnetic species in N-doped TiO_2 powders by EPR spectroscopy and DFT calculations," *Journal of Physical Chemistry B*, vol. 109, no. 23, pp. 11414–11419, 2005.

[14] S. P. Qiu and S. J. Kalita, "Synthesis, processing and characterization of nanocrystalline titanium dioxide," *Materials Science and Engineering A*, vol. 435-436, pp. 327–332, 2006.

[15] M. Kanna and S. Wongnawa, "Mixed amorphous and nanocrystalline TiO_2 powders prepared by sol-gel method: characterization and photocatalytic study," *Materials Chemistry and Physics*, vol. 110, no. 1, pp. 166–175, 2008.

[16] S. M. Oh, S. S. Kim, J. E. Lee, T. Ishigaki, and D. W. Park, "Effect of additives on photocatalytic activity of titanium dioxide powders synthesized by thermal plasma," *Thin Solid Films*, vol. 435, no. 1-2, pp. 252–258, 2003.

[17] X. H. Wang, J. G. Li, H. Kamiyama, and T. Ishigaki, "Fe-doped TiO_2 nanopowders by oxidative pyrolysis of organometallic precursors in induction thermal plasma: synthesis and structural characterization," *Thin Solid Films*, vol. 506-507, pp. 278–282, 2006.

[18] J. G. Li, X. H. Wang, H. Kamiyama, T. Ishigaki, and T. Sekiguchi, "RF plasma processing of Er-doped TiO_2 luminescent nanoparticles," *Thin Solid Films*, vol. 506-507, pp. 292–296, 2006.

[19] J. E. Lee, S. M. Oh, and D. W. Park, "Synthesis of nano-sized Al doped TiO_2 powders using thermal plasma," *Thin Solid Films*, vol. 457, no. 1, pp. 230–234, 2004.

[20] X. W Zhang, M. H. Zhou, and L. C. Lei, "Preparation of anatase TiO_2 supported on alumina by different metal organic chemical vapor deposition methods," *Applied Catalysis A*, vol. 282, no. 1-2, pp. 285–293, 2005.

[21] C. Z. Li, L. Y. Shi, D. M. Xie, and H. Du, "Morphology and crystal structure of A1-doped TiO_2 nanoparticles synthesized by vapor phase oxidation of titanium tetrachloride," *Journal of Non-Crystalline Solids*, vol. 352, no. 38-39, pp. 4128–4135, 2006.

[22] M. Q. Wang, B. Gong, X. Yao, Y. Wang, and R. N. Lamb, "Preparation and microstructure properties of Al-doped TiO_2-SiO_2 gel-glass film," *Thin Solid Films*, vol. 515, no. 4, pp. 2055–2058, 2006.

[23] Y. J. Choi, Z. Seeley, A. Bandyopadhyay, S. Bose, and S. A. Akbar, "Aluminum-doped TiO_2 nano-powders for gas sensors," *Sensors and Actuators B*, vol. 124, no. 1, pp. 111–117, 2007.

[24] C. Y. Tsai, H. C. Hsi, H. Bai, K. S. Fan, and C. Chen, "TiO_{2-x} nanoparticles synthesized using He/Ar thermal plasma and their effectiveness on low-concentration mercury vapor removal," *Journal of Nanoparticle Research*, vol. 13, no. 10, pp. 4739–4748, 2011.

[25] C. Y. Tsai, H. C. Hsi, H. Bai, K. S. Fan, and H. D. Sun, "Novel synthesis of Al-doped TiO_2 nanoparticles by direct combination of aluminum, titanium and oxygen using thermal plasma torch," *Japan Journal of Applied Physics*, vol. 51, p. 01AL01-1-6, 2012.

[26] R. A. Spurr, "Quantitative analysis of anatase-rutile mixtures with an X-ray diffractometer," *Analytical Chemistry*, vol. 29, no. 5, pp. 760–762, 1957.

[27] S. Karvinen, "The effects of trace elements on the crystal properties of TiO_2," *Solid State Sciences*, vol. 5, no. 5, pp. 811–819, 2003.

[28] M. L. Taylor, G. E. Morris, and R. S. Smart, "Influence of aluminum doping on titania pigment structural and dispersion properties," *Journal of Colloid and Interface Science*, vol. 262, no. 1, pp. 81–88, 2003.

[29] B. Y. Lee, S. H. Park, M. S. Kang, S. C. Lee, and S. J. Choung, "Preparation of Al/TiO_2 nanometer photo-catalyst film and the effect of H_2O addition on photo-catalytic performance for benzene removal," *Applied Catalysis A*, vol. 253, no. 2, pp. 371–380, 2003.

[30] H. K. Shon, D. L. Cho, S. H. Na, J. B. Kim, H. J. Park, and J. H. Kim, "Development of a novel method to prepare Fe- and Al-doped TiO_2 from wastewater," *Journal of Industrial and Engineering Chemistry*, vol. 15, no. 4, pp. 476–482, 2009.

[31] I. Nakamura, N. Negishi, S. Kutsuna, T. Ihara, S. Sugihara, and K. Takeuchi, "Role of oxygen vacancy in the plasma-treated TiO_2 photocatalyst with visible light activity for NO removal," *Journal of Molecular Catalysis A*, vol. 161, no. 1-2, pp. 205–212, 2000.

[32] C. T. Wang and S. H. Ro, "Nanoparticle iron-titanium oxide aerogels," *Materials Chemistry and Physics*, vol. 101, no. 1, pp. 41–48, 2007.

[33] M. Steveson, T. Bredow, and A. R. Gerson, "MSINDO quantum chemical modelling study of the structure of aluminium-doped anatase and rutile titanium dioxide," *Physical Chemistry Chemical Physics*, vol. 4, no. 2, pp. 358–365, 2002.

[34] U. Gesenhues and T. Rentschler, "Crystal growth and defect structure of Al^{3+}-doped rutile," *Journal of Solid State Chemistry*, vol. 143, no. 2, pp. 210–218, 1999.

[35] W. J. Zhang, Y. Li, S. L. Zhu, and F. H. Wang, "Copper doping in titanium oxide catalyst film prepared by dc reactive magnetron sputtering," *Catalysis Today*, vol. 93-95, pp. 589–594, 2004.

[36] Y. Li, P. Murphy, and C. Y. Wu, "Removal of elemental mercury from simulated coal-combustion flue gas using a SiO_2-TiO_2 nanocomposite," *Fuel Processing Technology*, vol. 89, no. 6, pp. 567–573, 2008.